Analysis of masonry structures with damage models

Francisco Natário

M.Sc. thesis summary

Abstract

The main objective of the present work is to test the numerical performance of non-conventional finite element formulations using continuum damage models, in order to describe the structural behavior of masonry structures.

Only isotropic and continuum damage models are considered. Linear geometrically analysis are performed, not considering permanent deformations.

Two non-conventional formulations are tested: the hybrid-mixed stress formulation with effective stress approximation and the hybrid-displacement. Three damage models are implemented within the hybrid-mixed stress formulation. Only one of the three damage models is implemented within the hybrid-displacement formulation. One of the three damage models is implemented within the hybrid-mixed stress formulation for the first time.

Even though the damage models have not been calibrated, the effectiveness os such modeling strategies is discussed from a qualitative point of view. Important conclusions can be taken from the case studies, which were masonry shear walls and a cilindrical vault.

1 Introduction

Masonry is one of the oldest building materials that still finds wide use in today's building industries. Moreover, the preservation of the architectural heritage is considered a fundamental issue and the research interest in this area has begun to increase.

Masonry is a heterogeneous material composed of units assembled by dry or mortar joints. Stones, ashlars, adobes and bricks have been used as units, which can be joined together using mortar or just by simple superposition. With these two components, units and joints, a large number of arrangements can be carried out. Nevertheless, the mechanical behavior of different types of masonry exhibits generally a very low tensile strength. This property is so important that it has determined the structural form of historical constructions.

Safety assessment and the evaluation of restoration actions to be performed on masonry constructions demands the development of modeling tools, able to effectively represent the response of masonry.

Most of the existing studies on masonry behavior are based on the following methods Gago [2004]:

- classical approach, i.e., limit analysis;
- numerical modeling, often based on finite element methods.

In the framework of the numerical modeling three main approaches can be used: the micro-modeling of single components (e.g., units and mortar), the macro-modeling of the masonry as a continuum material, and the discrete element method.

The first approach can be profitably used for the detailed modeling of particular elements of the structure. On the other hand, for large structures, such an approach involves an enormous computational effort, usually not justifiable. The macro approach appears to be enough to reproduce the behavior of

large masonry structures. However, [Lourenço, 1996] demonstrated that a macro-modeling strategy can perform badly, when used in cases where the failure mode is governed by the interaction of a few units and mortar.

In any case, the modeling of masonry structures needs to take into account their semi-discrete and composite nature. In addition, an adequate computational model should include the fundamental mechanisms that characterize the masonry behavior at failure. The failure mechanism of the components loaded in tension and compression is essentially the same, viz. crack growth at the microlevel of the material. In this process inelastic strains result from a dissipative process in which fracture energy is released during the process of internal fracture. The composite material shows, however, another type of failure, sliding or mode II, which results in a dry friction process between the components once softening is completed [Lourenço, 1996]. If a micro-modeling strategy is used all these phenomena can be incorporated in the model because joints and units are represented separately. In a macro-modeling strategy joints are smeared out in a homogeneous continuum, and the interaction between the components cannot be incorporated in the model. Instead, a relation between average stresses and strains is established.

Independently of the type of strategy adopted, accurate masonry models can only be used if a complete material description is available. Unfortunately, this is not the case, and experimental data suitable for numerical purpose are scarce, especially in softening regime.

In the context of macro approach the usual numerical modeling strategies can be adopted, such as classical plasticity theory, damage approach, etc.

In this study the damage theory has been adopted. It has been revealed to be a good choice to exploit in this area of structural mechanics (e.g. [Creazza et al., 2002; Oñate et al., 1996]), due especially to its efficiency combined with simplicity.

Unlike the works published by [Creazza et al., 2002, 2001], non-conventional finite elements are used in this study, instead of the traditional displacement finite element method.

The non-conventional hybrid and mixed formulations had a significant development with the work of [Freitas, 1989], [Freitas et al., 1999], [Castro, 1996], among others. [Silva, 2006] has developed a pioneering work by bringing up together non-conventional hybrid and mixed formulations and continuum damage mechanics, in order to study the non-linear behavior of 2D concrete structures. In this work the hybrid-mixed stress formulation and the hybrid-displacement formulation are used, with the software developed by [Silva, 2006].

The hybrid-mixed stress models are based on the direct and independent approximation of the stress and displacement fields in the domain of each element. The displacements on the static boundary, which includes the boundaries shared by two elements, are also approximated independently. None of the fundamental relations are locally enforced *a priori*. All field equations are imposed in a weighted residual form, ensuring that the discrete numerical model embodies all the relevant properties of the continuum fields it represents. This finite element formulation is defined as a stress model since the equilibrium conditions on the boundary are used to enforce on average the continuity conditions between elements. From a structural engineering point of a view, the main advantage of this numerical model is that *quasi*-equilibrated solutions are locally obtained. Unfortunately, the classic version of the hybrid-mixed stress formulation does nor provide enough information to define univocally the evolution of damage in the material. In order to overcome this fact, [Silva, 2006] has developed a hybrid-mixed stress model that replaces the approximation of the stress field in the domain of each finite element by an independent approximation of the effective stress field.

The hybrid-displacement models are based on the direct approximation of the displacement fields in the domain of each element. The continuity between elements is imposed in a weighted-residual form using the compatibility equation on the Dirichlet boundary (which include inter-element boundaries), so the tractions on the Dirichlet boundary are also independently approximated. Because the compatibility is enforced between elements, the adopted model is defined as a displacement formulation.

2 Fundamental relations

Consider a domain V, limited by the boundary Γ, referred to a cartesian coordinate system. The static boundary Γ_σ and the kinematic boundary Γ_u (or Dirichlet boundary) are complementary sub-regions of the boundary Γ, whereon traction-resultants and displacements are respectively prescribed. We only consider static loads including the body-force vector $\mathbf{b}$ in the domain V, the vector $\mathbf{t}_\gamma$ on the boundary Γ_σ and the imposed displacements on the kinematic boundary Γ_u, defined in vector $\overline{\mathbf{u}}$. The body under analysis is assumed to be isotropic, i.e., the material properties are the same in all directions. The model is geometrically linear but the behavior of the material is nonlinear.

2.1 Equilibrium and compatibility equations

The fundamental equilibrium equations may be written in a matrix form as follows:

$$\mathbf{D}\sigma + \mathbf{b} = 0 \qquad \text{in } V, \tag{1}$$

$$\mathbf{N}\sigma = \mathbf{t}_\gamma \qquad \text{on } \Gamma_\sigma, \tag{2}$$

where $\mathbf{D}$ is the differential equilibrium operator. The matrix $\mathbf{N}$ lists the components of the unit outward normal vector to the static boundary Γ_σ associated with $\mathbf{D}$. The vector σ lists the independent components of the stress tensor. The vector $\mathbf{b}$ represents the body-force vector in the domain V and $\mathbf{t}_\gamma$ corresponds to the tractions vector on the static boundary Γ_σ. For plane elasticity problems, these vectors are defined as follows:

$$\sigma = \begin{bmatrix} \sigma_{xx} \\ \sigma_{yy} \\ \sigma_{xy} \end{bmatrix}, \quad \mathbf{b} = \begin{bmatrix} \mathbf{b}_x \\ \mathbf{b}_y \end{bmatrix}, \quad \mathbf{t}_\gamma = \begin{bmatrix} \mathbf{t}_{x\gamma} \\ \mathbf{t}_{y\gamma} \end{bmatrix}. \tag{3}$$

The compatibility equations may be written in the following format:

$$\varepsilon = \mathbf{D}^*\mathbf{u} \qquad \text{in } V, \tag{4}$$

$$\mathbf{u} = \bar{\mathbf{u}} \qquad \text{on } \Gamma_u, \tag{5}$$

where $\mathbf{D}^*$ is the differential compatibility operator (adjoint of the differential equilibrium operator $\mathbf{D}$ since the model is geometrically linear). The vector ε collects the independent components of the strain tensor and the vector $\mathbf{u}$ lists the independent components of the displacements. The prescribed displacements along the kinematic boundary are listed in vector $\overline{\mathbf{u}}$. For a plane elasticity problem, these vectors may be written as follows:

$$\varepsilon = \begin{bmatrix} \varepsilon_{xx} \\ \varepsilon_{yy} \\ \gamma_{xy} \end{bmatrix}, \quad \mathbf{u} = \begin{bmatrix} \mathbf{u}_x \\ \mathbf{u}_y \end{bmatrix}, \quad \overline{\mathbf{u}} = \begin{bmatrix} \overline{\mathbf{u}}_x \\ \overline{\mathbf{u}}_y \end{bmatrix}. \tag{6}$$

2.2 Constitutive relation

Three damage models have been implemented in this work. Two of them were presented by [Comi and Perego, 2001b,a] and implemented by [Silva, 2006]. The third model was first published by Mazars [1984], and its implementation combined with non-conventional finite elements has never been done before.

2.2.1 Constitutive relation with one damage variable [Comi and Perego, 2001b]

The authors define the following state equations:

$$\sigma = (\mathbf{1} - \mathbf{d})\mathbf{K}\varepsilon; \quad \mathbf{Y} = \frac{\mathbf{1}}{\mathbf{2}}\varepsilon^t\mathbf{K}\varepsilon; \quad \chi = \mathbf{k}\ln^n\frac{\mathbf{c}}{\mathbf{1}-\xi}, \tag{7}$$

where the state variables are the elastic strain ε, the damage variable $\mathbf{d}$ an the internal variable ξ. The associated variables are the stress σ, the elastic energy release rate $\mathbf{Y}$ and the variable χ. The parameters $\mathbf{k}$, $\mathbf{n}$, $\mathbf{c}$ and the elastic tensor of the virgin material $\mathbf{K}$ are material properties.

The evolution laws are obtained from the loading function $\mathbf{f}$ (or potencial of dissipation). Equation (8) defines the the loading function and the loading-unloading conditions for the present model:

$$\mathbf{f}(\mathbf{Y} - \chi) = \mathbf{Y} - \chi = \frac{\mathbf{1}}{\mathbf{2}}\varepsilon^t\mathbf{K}\varepsilon - \chi \leq \mathbf{0}; \quad \dot{\gamma} \geq \mathbf{0}; \quad \mathbf{f}\dot{\gamma} = \mathbf{0}, \tag{8}$$

where γ represents a positive scalar.

The associative evolution laws of the internal variables may be written in the following form:

$$\dot{\mathbf{d}} = \frac{\partial \mathbf{f}}{\partial \mathbf{Y}}\dot{\gamma} = \dot{\gamma}; \quad \dot{\xi} = -\frac{\partial \mathbf{f}}{\partial \chi}\dot{\gamma} = \dot{\gamma}. \tag{9}$$

Using Equation (9), it is easy to conclude that, for this particular damage model, the internal variable ξ coincides with the the damage variable $\mathbf{d}$.

It is possible to define an effective stress vector, $\widetilde{\sigma}$, that depends on the stress field σ and on the damage variable $\mathbf{d}$. To simplify the presentation, we assume that $\widetilde{\sigma} = \sigma(\mathbf{1} - \mathbf{d})$, but the model is easily generalized for a more complicated relations. Using this definition, the potencial of dissipation can be written on the following form:

$$\mathbf{f}(\mathbf{Y} - \chi) = \mathbf{Y} - \chi = \frac{\mathbf{1}}{\mathbf{2}}\widetilde{\sigma}^t\mathbf{F}\widetilde{\sigma} - \chi, \tag{10}$$

where $\mathbf{F}$ represents the elastic flexibility matrix of the virgin material.

In a one-dimensional case, the damage model assumes a linear elastic behavior until strain reaches its linear limit, $\varepsilon_0 = \sqrt{\mathbf{k}ln(c)^n}\frac{\mathbf{2}}{\mathbf{E}}$. From this point forward, the damage variable is larger than zero and the material's behavior is nonlinear. It is important to notice that the constitutive model adopted has the limitation of considering the same behavior for the material in prevailing tension and compression. To overcome this limitation, it is assumed that damage can only occur if $tr(\varepsilon) \geq 0$.

2.2.2 Constitutive relation with two damage variables [Comi and Perego, 2001a]

The damage model presented by [Comi and Perego, 2001a] assumes that the nonlinear behavior of the material is controlled by two different mechanisms: one for tension (t) and the other for compression (c). The authors define two independent damage variables, $\mathbf{d}_t$ and $\mathbf{d}_c \in [0, 1[$.

The constitutive relation in this model is given by:

$$\sigma = \mathbf{2}\mu\mathbf{e} + \mathbf{k}_+(\mathbf{tr}^+\varepsilon)\mathbf{I} + \mathbf{k}_-(\mathbf{tr}^-\varepsilon)\mathbf{I}, \tag{11}$$

where

$$\mu = \mu_0(\mathbf{1} - \mathbf{d}_t)(\mathbf{1} - \mathbf{d}_c), \quad \mathbf{e} = \varepsilon - \frac{\mathbf{tr}(\varepsilon)}{\mathbf{3}}\mathbf{I}, \quad \mathbf{tr}^+(\varepsilon) = \frac{\mathbf{tr}(\varepsilon) + |\mathbf{tr}(\varepsilon)|}{\mathbf{2}}, \quad \mathbf{tr}^-(\varepsilon) = \frac{\mathbf{tr}(\varepsilon) - |\mathbf{tr}(\varepsilon)|}{\mathbf{2}},$$
$$\mathbf{k}_+ = \mathbf{k}_0(\mathbf{1} - \mathbf{d}_t) \text{ if } \mathbf{tr}^+(\varepsilon) \geq 0, \quad \mathbf{k}_- = \mathbf{k}_0(\mathbf{1} - \mathbf{d}_c) \text{ if } \mathbf{tr}^-(\varepsilon) < 0.$$

The material properties μ_0 and $\mathbf{k}_0$ are, respectively, the shear modulus and the compressive modulus of the virgin material. The identity matrix is represented by $\mathbf{I}$.

The loading functions written in terms of the effective stress field are:

$$\begin{cases} \mathbf{f}_t = [(\mathbf{1}-\mathbf{d}_t)(\mathbf{1}-\mathbf{d}_c)]^2\mathbf{J}_{\widetilde{\sigma}} - \mathbf{a}_t[(\mathbf{1}-\mathbf{d}_t)\mathbf{tr}^+(\widetilde{\sigma}) + (\mathbf{1}-\mathbf{d}_c)\mathbf{tr}^-(\widetilde{\sigma})]^2 \\ \qquad +\mathbf{b}_t\mathbf{r}_t[(\mathbf{1}-\mathbf{d}_t)\mathbf{tr}^+(\widetilde{\sigma}) + (\mathbf{1}-\mathbf{d}_c)\mathbf{tr}^-(\widetilde{\sigma})] - \mathbf{k}_t{\mathbf{r}_t}^2(\mathbf{1}-\alpha\mathbf{d}_c) \\ \mathbf{f}_c = [(\mathbf{1}-\mathbf{d}_t)(\mathbf{1}-\mathbf{d}_c)]^2\mathbf{J}_{\widetilde{\sigma}} + \mathbf{a}_c[(\mathbf{1}-\mathbf{d}_t)\mathbf{tr}^+(\widetilde{\sigma}) + (\mathbf{1}-\mathbf{d}_c)\mathbf{tr}^-(\widetilde{\sigma})]^2 \\ \qquad +\mathbf{b}_c\mathbf{r}_c[(\mathbf{1}-\mathbf{d}_t)\mathbf{tr}^+(\widetilde{\sigma}) + (\mathbf{1}-\mathbf{d}_c)\mathbf{tr}^-(\widetilde{\sigma})] - \mathbf{k}_c{\mathbf{r}_c}^2 \end{cases} \tag{12}$$

where $\mathbf{J}_{\widetilde{\sigma}} = \frac{\mathbf{1}}{\mathbf{2}}\widetilde{\mathbf{s}}^t\widetilde{\mathbf{s}}$ represents the second invariant of the efective stress deviator tensor $\widetilde{\mathbf{s}}$ and $\mathbf{a}_t$, $\mathbf{b}_t$, $\mathbf{k}_t$, $\mathbf{a}_c$, $\mathbf{b}_c$, $\mathbf{k}_c$ and α are non-negative material parameters. Functions $\mathbf{r}_c$ and $\mathbf{r}_t$ are used to define the damage evolution laws, which can be defined by:

$$\mathbf{r}_i(\mathbf{d}_i) = \begin{cases} \mathbf{1} - \frac{\mathbf{1}-(\frac{\sigma_e}{\sigma_0})_i}{{\mathbf{d}_{0i}}^2}(\mathbf{d}_{0i}-\mathbf{d}_i)^2, & \mathbf{d}_i < \mathbf{d}_{0i} \\ \{\mathbf{1} - (\frac{\mathbf{d}_i-\mathbf{d}_{0i}}{\mathbf{1}-\mathbf{d}_{0i}})^{c_i}\}^{0.75}, & \mathbf{d}_i \geq \mathbf{d}_{0i} \end{cases} \qquad \mathbf{i} = \mathbf{t}, \mathbf{c}, \tag{13}$$

where $\mathbf{d}_{0i}$ represents the value of the damage variable in an uniaxial stress-strain peak associated to $\sigma = \sigma_{0i}$ and the parameter $\mathbf{c}_i$ controls the softening curve of the stress-strain relation. The limit value of the elastic stress is given by σ_{ei}, where i represents tension (t) or compression (c). It is also important to notice that the term $(\mathbf{1}-\alpha\mathbf{d}_c)$ of the loading function for tension stress states allows to model the decrease of tension strength if compression damage occurs.

2.2.3 Constitutive relation with one damage variable [Mazars, 1984]

The damage model presented by [Mazars, 1984] assumes that damage can occur only for tensile strains. The equivalent strain is a function of the principal strains, and can be determined as follows:

$$\widetilde{\varepsilon} = \sqrt{{\langle\varepsilon_I\rangle_+}^2 + {\langle\varepsilon_{II}\rangle_+}^2 + {\langle\varepsilon_{III}\rangle_+}^2} = \sqrt{\sum_{i=I}^{i=III}{\langle\varepsilon_i\rangle_+}^2}, \tag{14}$$

where $\langle(\cdot)\rangle_+ = \frac{1}{2}[(\cdot) + |(\cdot)|]$ and $\langle(\cdot)\rangle_- = \frac{1}{2}[(\cdot) - |(\cdot)|]$.

Damage occurs when the equivalent strain is greater than the strain $\varepsilon_{d0} = \frac{\mathbf{f}_t}{\mathbf{E}}$, where $\mathbf{f}_t$ is the uniaxial tensile strength for the material.

The loading function in this model is given by:

$$\mathbf{f}(\widetilde{\varepsilon}, \mathbf{d}) = \widetilde{\varepsilon} - \chi(\mathbf{d}) \leq \mathbf{0} \quad \text{with } \chi(\mathbf{0}) = \varepsilon_{d0}. \tag{15}$$

The damage evolution law can be written as follows:

$$\dot{\mathbf{d}} = \mathbf{0} \text{ if } \mathbf{f} < \mathbf{0} \text{ or } \mathbf{f} = 0 \text{ and } \dot{\mathbf{f}} < \mathbf{0}; \tag{16}$$

$$\dot{\mathbf{d}} = \mathbf{F}(\widetilde{\varepsilon})\langle\dot{\widetilde{\varepsilon}}\rangle_+ \text{ if } \mathbf{f} = \mathbf{0} \text{ and } \dot{\mathbf{f}} = \mathbf{0}, \tag{17}$$

The damage model presented by [Mazars, 1984] defines two internal damage variables, $\mathbf{d}_t$ e $\mathbf{d}_c$, which represent the tension and the compression damage. The evolution laws for these two variables are given by:

$$\dot{\mathbf{d}}_t = \mathbf{F}_t(\widetilde{\varepsilon})\langle\dot{\widetilde{\varepsilon}}\rangle_+; \tag{18}$$

$$\dot{\mathbf{d}}_c = \mathbf{F}_c(\widetilde{\varepsilon})\langle\dot{\widetilde{\varepsilon}}\rangle_+, \tag{19}$$

where:

$$\mathbf{F}_t(\widetilde{\varepsilon}) = \frac{\varepsilon_{d0}(\mathbf{1}-\mathbf{A}_t)}{\widetilde{\varepsilon}^2} + \frac{\mathbf{A}_t\mathbf{B}_t}{\exp[\mathbf{B}_t(\widetilde{\varepsilon}-\varepsilon_{d0})]}; \tag{20}$$

$$\mathbf{F}_c(\widetilde{\varepsilon}) = \frac{\varepsilon_{d0}(\mathbf{1}-\mathbf{A}_c)}{\widetilde{\varepsilon}^2} + \frac{\mathbf{A}_c\mathbf{B}_c}{\exp[\mathbf{B}_c(\widetilde{\varepsilon}-\varepsilon_{d0})]}. \tag{21}$$

The damage variables $\mathbf{d}_t$ e $\mathbf{d}_c$ can be written as follows:

$$\mathbf{d}_t(\widetilde{\varepsilon}) = \mathbf{1} - \frac{\varepsilon_{d0}(\mathbf{1}-\mathbf{A}_t)}{\widetilde{\varepsilon}} + \frac{\mathbf{A}_t}{\exp[\mathbf{B}_t(\widetilde{\varepsilon}-\varepsilon_{d0})]}; \tag{22}$$

$$\mathbf{d}_c(\widetilde{\varepsilon}) = \mathbf{1} - \frac{\varepsilon_{d0}(\mathbf{1}-\mathbf{A}_c)}{\widetilde{\varepsilon}} + \frac{\mathbf{A}_c}{\exp[\mathbf{B}_c(\widetilde{\varepsilon}-\varepsilon_{d0})]}. \tag{23}$$

$\mathbf{A}_t$, $\mathbf{B}_t$, $\widetilde{\varepsilon}_{d0}$,$\mathbf{A}_c$ and $\mathbf{B}_c$ are parameters of the material.
Finally, the damage variable is given by:

$$\mathbf{d} = \alpha_t\mathbf{d}_t + \alpha_c\mathbf{d}_c. \tag{24}$$

The parameters α_t and α_c can be computed using the following equations:

$$\alpha_t = \frac{\sum_i \langle\varepsilon_{T_i}\rangle_+}{\sum_i \langle\varepsilon_{T_i}\rangle_+ + \sum_i \langle\varepsilon_{C_i}\rangle_+}; \tag{25}$$

$$\alpha_c = \frac{\sum_i \langle\varepsilon_{C_i}\rangle_+}{\sum_i \langle\varepsilon_{T_i}\rangle_+ + \sum_i \langle\varepsilon_{C_i}\rangle_+}, \tag{26}$$

where:

$$\varepsilon_T = \frac{\mathbf{1}+\nu}{\mathbf{E}}\langle\widetilde{\sigma}\rangle_+ - \frac{\nu}{\mathbf{E}}\sum_i \langle\widetilde{\sigma}_i\rangle_+\mathbf{I}; \tag{27}$$

$$\varepsilon_C = \frac{\mathbf{1}+\nu}{\mathbf{E}}\langle\widetilde{\sigma}\rangle_- - \frac{\nu}{\mathbf{E}}\sum_i \langle\widetilde{\sigma}_i\rangle_-\mathbf{I}. \tag{28}$$

$\mathbf{I}$ represents the identity matrix, and $\langle\widetilde{\sigma}\rangle_+$ and $\langle\widetilde{\sigma}\rangle_-$ are the positive and negative members of the principal effective stress tensor.

3 Hybrid-mixed stress model

One of the two finite element formulations adopted in this work is based on the hybrid-mixed stress model described in [Silva, 2006]. The approximations may be expressed as:

$$\widetilde{\sigma} = \mathbf{S}\widetilde{\mathbf{X}} \quad \text{in } V, \quad \mathbf{u} = \mathbf{U}_v\mathbf{q}_v \quad \text{in } V, \quad \mathbf{u} = \mathbf{U}_\gamma\mathbf{q}_\gamma \quad \text{on } \Gamma_\sigma, \tag{29}$$

where the matrices $\widetilde{\mathbf{S}}$, $\mathbf{U}_v$ and $\mathbf{U}_\gamma$ collect the approximation functions and the vectors $\widetilde{\mathbf{X}}$, $\mathbf{q}_v$ and $\mathbf{q}_\gamma$ list the associated generalized variables. Since the three fields are approximated independently, it is possible to adopt different degrees of approximation for each one.

The $\mathbf{U}_v\{\mathbf{U}_\gamma\}$ average enforcement of the equilibrium equations in the domain {static boundary} leads to:

$$\int \mathbf{U}_v{}^t \mathbf{D}\widetilde{\sigma} dV - \int \mathbf{U}_v{}^t \mathbf{D}(\widetilde{\sigma} \times \mathbf{d}) dV + \int \mathbf{U}_v{}^t \mathbf{b} dV = 0, \tag{30}$$

$$\int \mathbf{U}_\gamma{}^t \mathbf{N}\widetilde{\sigma} d\Gamma_\sigma - \int \mathbf{U}_\gamma{}^t \mathbf{N}(\widetilde{\sigma} \times \mathbf{d}) d\Gamma_\sigma + \int \mathbf{U}_\gamma{}^t \mathbf{t}_\gamma d\Gamma_\sigma = 0. \tag{31}$$

Replacing the approximation for the effective stress field in the domain (Equation (29)) in Equations (30) and (31), and integrating by parts the second term of the equilibrium in the domain, one obtains the equilibrium equations for the discrete model:

$$(\mathbf{A}_v{}^t - \mathbf{M}_1)\widetilde{\mathbf{X}} = -\mathbf{Q}_v \quad \text{in } V, \tag{32}$$

$$(\mathbf{A}_\gamma{}^t - \mathbf{M}_2)\widetilde{\mathbf{X}} = -\mathbf{Q}_\gamma \quad \text{on } \Gamma_\sigma, \tag{33}$$

where the matrices $\mathbf{M}_1$, $\mathbf{M}_2$, $\mathbf{A}_v$, $\mathbf{A}_\gamma$ and the vectors $\mathbf{Q}_v$ and $\mathbf{Q}_\gamma$ are defined as follows:

$$\mathbf{M}_1 = -\int (\mathbf{D}^* \mathbf{U}_v)^t \mathbf{S}\mathbf{d} dV + \int (\mathbf{N}^* \mathbf{U}_v)^t \mathbf{S}\mathbf{d} d\Gamma_\sigma, \quad \mathbf{M}_1 = \int \mathbf{U}_\gamma{}^t (\mathbf{N}\mathbf{S})\mathbf{d} d\Gamma_\sigma, \tag{34}$$

$$\mathbf{A}_v = \int (\mathbf{D}\mathbf{S})^t \mathbf{U}_v dV, \quad \mathbf{A}_\gamma = \int (\mathbf{N}\mathbf{S})^t \mathbf{U}_\gamma d\Gamma_\sigma, \tag{35}$$

$$\mathbf{Q}_v = \int \mathbf{U}_v^t \mathbf{b} dV, \quad \mathbf{Q}_\gamma = \int \mathbf{U}_\gamma^t \mathbf{t}_\gamma d\Gamma_\sigma. \tag{36}$$

The compatibility condition in the discrete model may be obtained integrating by parts the **S**-average enforcement of the compatibility equation in the domain and then replacing in the resulting expression the approximations for the displacements (Equation (29)):

$$\int \mathbf{S}^t \varepsilon dV = -\mathbf{A}_v \mathbf{q}_v + \mathbf{A}_v \mathbf{q}_\gamma + \overline{\mathbf{e}} \quad \text{with } \overline{\mathbf{e}} = \int (\mathbf{N}\mathbf{S})^t \overline{\mathbf{u}} d\Gamma_u. \tag{37}$$

Introducing the constitutive relation in Equation (37), we obtain Equation (38) that englobes simultaneously the compatibility and the constitutive relations of the discrete model:

$$\mathbb{F}\widetilde{\mathbf{X}} + \mathbf{A}_v \mathbf{q}_v - \mathbf{A}_\gamma \mathbf{q}_\gamma \quad \text{with } \mathbb{F} = \int \mathbf{S}^t \mathbf{F} \mathbf{S} dV. \tag{38}$$

The solving system for each finite element is constructed by combining Equations (32), (33) and (38):

$$\begin{bmatrix} \mathbb{F} & \mathbf{A}_v & -\mathbf{A}_\gamma \\ (\mathbf{A}_v{}^t - \mathbf{M}_1) & \mathbf{0} & \mathbf{0} \\ -(\mathbf{A}_\gamma{}^t - \mathbf{M}_2) & \mathbf{0} & \mathbf{0} \end{bmatrix} \begin{bmatrix} \widetilde{\mathbf{X}} \\ \mathbf{q}_v \\ \mathbf{q}_\gamma \end{bmatrix} = \begin{bmatrix} \overline{\mathbf{e}} \\ -\mathbf{Q}_v \\ -\mathbf{Q}_\gamma \end{bmatrix}. \tag{39}$$

The governing system of the finite element mesh is assembled by direct allocation of the contribution of the elementary systems.

When damage mechanism in a finite element is active, the elementary governing system is non-symmetric.

4 Hybrid-displacement model

The other finite element formulation adopted in this work is based on the hybrid-displacement model described in [Silva, 2006]. The approximations may be expressed as:

$$\mathbf{u} = \mathbf{U}_v \mathbf{q} \quad \text{in } V, \quad \mathbf{t} = \mathbf{T}\mathbf{p} \quad \text{on } \Gamma_u, \tag{40}$$

where the matrices $\mathbf{U}_v$ and $\mathbf{T}$ collect the approximation functions and the vectors $\mathbf{q}$ and $\mathbf{p}$ list the associated generalized variables.

Imposing that the energy dissipated by the discrete variables is equal to the one dissipated by the continuum fields they represent, it is possible to define the generalized displacements $\mathbf{v}$ and the generalized body-forces $\mathbf{Q}_v$:

$$\mathbf{v} = \int \mathbf{T}^t \overline{\mathbf{u}} d\Gamma_u, \quad \mathbf{Q}_v = \int \mathbf{U}_v^t \mathbf{b} dV. \tag{41}$$

The equilibrium in the domain and the compatibility on the boundary Γ_u are enforced on average, in the sense of Galerkin, as follows:

$$\int \mathbf{U}_v^t (\mathbf{D}\sigma + \mathbf{b}) dV = 0, \tag{42}$$

$$\int \mathbf{T}^t (\mathbf{u} - \overline{\mathbf{u}}) d\Gamma_u = 0. \tag{43}$$

Introducing in Equation (42) the definition of the generalized body-forces $\mathbf{Q}_v$ (Equation (41)) and integrating by parts, we obtain:

$$-\int (\mathbf{D}^* \mathbf{U}_v)^t \sigma dV + \int (\mathbf{N}^* \mathbf{U}_v)^t \sigma d\Gamma_u + \int (\mathbf{N}^* \mathbf{U}_v)^t \sigma d\Gamma_\sigma = -\mathbf{Q}_v. \tag{44}$$

The equilibrium conditions in the discrete model are obtained by replacing the approximations fields (Equation (40)) in Equation (44), leading to:

$$\widetilde{\mathbb{K}}\mathbf{q} - \mathbf{B}\mathbf{p} = \mathbf{Q}_v + \mathbf{Q}_\Gamma \quad \text{in } V, \tag{45}$$

where

$$\widetilde{\mathbb{K}} = \int (\mathbf{D}^* \mathbf{U}_v)^t (\mathbf{1} - \mathbf{d}) \mathbf{K} (\mathbf{D}^* \mathbf{U}_v) dV, \tag{46}$$

$$\mathbf{B} = \int \mathbf{U}_v^t \mathbf{T} d\Gamma_u, \tag{47}$$

$$\mathbf{Q}_\Gamma = \int \mathbf{U}_v^t \mathbf{t}_\gamma d\Gamma_\sigma. \tag{48}$$

Replacing the approximations (Equation (40)) in Equation (43) it is easy to obtain the compatibility equation on the kinematic boundary Γ_u for the discrete model:

$$-\mathbf{B}^t \mathbf{q} = -\mathbf{v} \quad \text{on } \Gamma_u. \tag{49}$$

Combining Equations (45) and (49), we obtain the following solving system for each finite element:

$$\begin{bmatrix} \widetilde{\mathbb{K}} & -\mathbf{B} \\ -\mathbf{B}^T & \mathbf{0} \end{bmatrix} \begin{bmatrix} \mathbf{q} \\ \mathbf{p} \end{bmatrix} = \begin{bmatrix} \mathbf{Q}_v + \mathbf{Q}_\Gamma \\ -\mathbf{v} \end{bmatrix}. \tag{50}$$

The governing system of the finite element mesh is assembled by direct allocation of the contribution of each elementary system.

5 Implementation [Silva, 2006]

The approximation functions adopted are the orthogonal and hierarchical Legendre polynomials defined over a master element ($\xi, \eta \in [-1, 1]$).

In the hybrid-mixed stress formulation, the matrices $\mathbf{M}_1$ and $\mathbf{M}_2$ require the use of a numerical integration scheme, while in the hybrid-displacement formulation, only the matrix $\widetilde{\mathbb{K}}$ requires that kind of algorithm. Lobatto's quadrature rules ([Pereira, 1993]) are used when numerical integration is required.

A finite element analysis of materials with softening behavior is well known lo localize strains in a vanishing volume, leading to unrealistic solutions associated with zero dissipation. From a mathematical point of view, it may be stated that the boundary value problem describing the structural response becomes ill-posed. In order to restore the well-posedness of this problem, a non-local integral formulation is adopted, considering a weighted average over the whole domain of the energy release rate when the constitutive relation with one damage variable of [Comi and Perego, 2001b] is used. When the two damage model of [Comi and Perego, 2001a] is adopted, the effective stress tensor's invariants are the weighted parameters. Finally, in [Mazars, 1984] damage model, the equivalent strain is the chosen parameter.

During the iterative procedure, the Lobatto points are used for two purposes. On one hand, in the non-local model, they are used to calculate the non-local variable, while on the other hand they are used in the numerical integration.

In order to solve the non-linear problem, a secant Newton-Raphson method is used.

Detailed information about the algorithms used can be found in [Silva, 2006] or [Silva and Castro, 2007].

6 Numerical examples

6.1 TU Eindhoven shear walls

Tests on masonry shear walls were carried out in the Technische Universiteit Eindhoven (TU Eindhoven). The shear walls have a width/height ratio of one with dimensions of $1000 \times 1000[mm^2]$. The walls are made of wire-cut solid clay bricks with dimensions $210 \times 52 \times 100[mm^3]$. Different vertical precompression uniformly distributed forces are applied to the walls, before a horizontal load is monotonically increased under top displacement control in a confined way, i.e. keeping the bottom and top boundaries horizontal and precluding any vertical movement.

In this thesis, it was not considered the precompression load and the wall self-weight, because the software used does not allow changes on the kinematic boundary during the loading process.

The deformed mesh obtained by [Lourenço, 1996] is illustrated in Figure 1. [Lourenço, 1996] used a micro-modeling strategy which has successfully reproduced the experimental data. The precompression load of this example is $0.30N/mm^2$, which is the nearest case to our example.

In this case, hybrid-mixed stress and hybrid-displacement models were used combined with [Comi and Perego, 2001b] one damage variable constitutive model. The damage model parameters adopted are $\mathbf{E} = 5700$MPa, $\nu = 0.25$, $k = 6.87 \times 10^{-6}$MPa, $c = 2.72$ and $n = 2.5$, resulting in the uniaxial tension

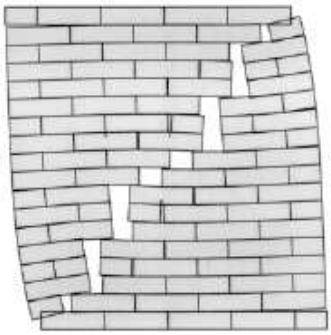

Figure 1: Deformed mesh for TU Eindhoven shear wall (results of micro-modeling strategy by [Lourenço, 1996]).

stress-strain relation presented in Figure 2. The degree of approximation of the effective stress field is 5, while 4 is used for the other fields approximated. The finite element mesh has only one element.

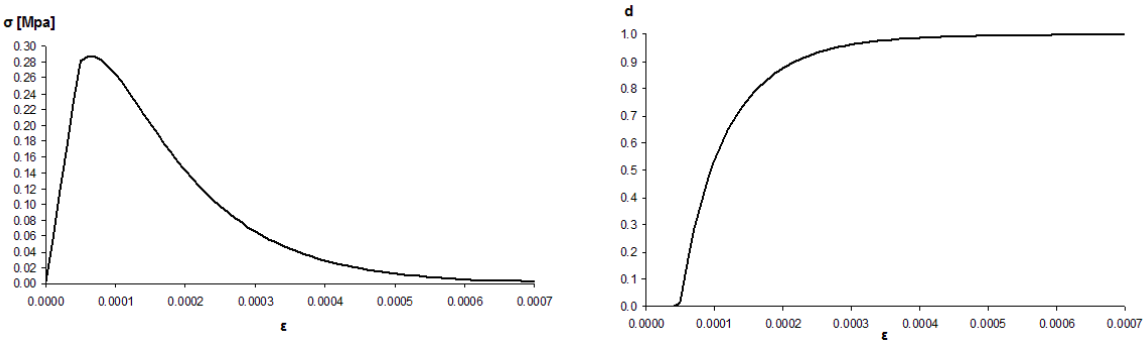

(a) stress-strain

(b) damage-strain

Figure 2: Constitutive relation adopted.

The load-displacement diagram obtained is shown in Figure 3, while the damage distribution obtained in both models is illustrated in Figure 4.

The phenomena responsible for the non-linearity of both load-displacement diagrams is the damage development in the bottom and top boundaries, corresponding to the observed cracks in experiments. However, the constitutive model is not suitable for this case study, because after the damage occurs, the structure is able to equilibrate the loading by means of a strut.

Another aspect that we should notice is that the hybrid-mixed stress model is more flexible than the hybrid-displacement model. This fact is easily perceptible, because it happens for pure stress and displacement models.

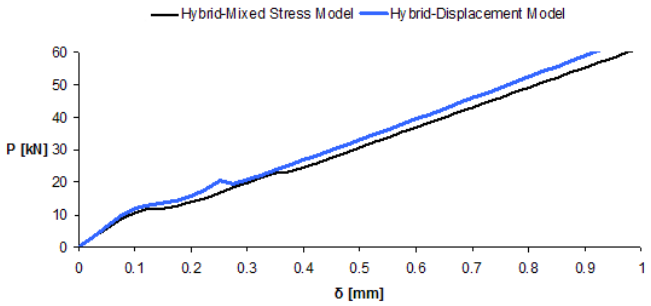

Figure 3: Load-displacement diagrams.

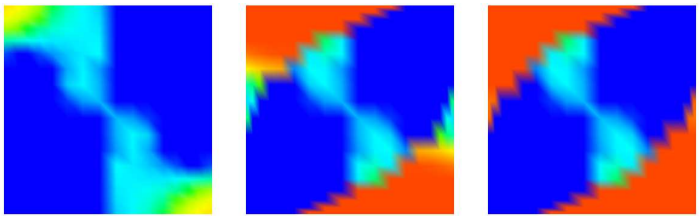

(a) HMSM $\delta = 0.10$mm (b) HMSM $\delta = 0.38$mm (c) HMSM $\delta = 1.00$mm

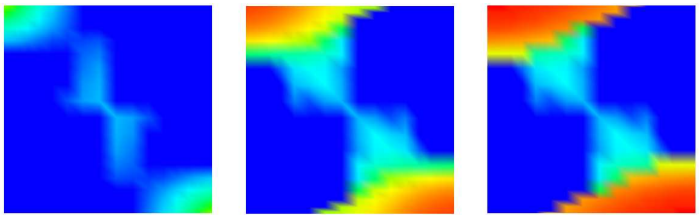

(d) HDM $\delta = 0.08$mm (e) HDM $\delta = 0.20$mm (f) HDM $\delta = 1.00$mm

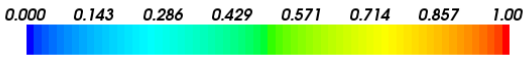

(g) colour scale

Figure 4: Damage distributions.

6.2 ETH Zurich shear walls

Tests on masonry shear walls were carried out in the Eigenössische Technische Hochsule Zürich (ETH Zurich). The shear walls have a width/height ratio of 1.8 with dimensions of $3600 \times 2000 \times 150[mm^3]$. The walls are made of hollow clay bricks. A vertical precompression uniformly distributed force ($0.62N/mm^2$) is applied to the wall, before a horizontal load is monotonically increased under top displacement control in a confined way, i.e. keeping the bottom and top boundaries horizontal and precluding any vertical movement. This wall was classified by [Lourenço, 1996] as "suitable" for a continuum analysis, because its global behavior is not dependent on the behavior of few units and joints.

The degree of approximation of the effective stress field is 5, while 4 is used for the other fields approximated. The mesh used has four equal rectangular finite elements.

[Mazars, 1984] damage model was adopted with the parameters $\mathbf{E} = 5700$MPa, $\nu = 0.25$, $\varepsilon_{d0} = 4.91x10^{-5}$, $\mathbf{A}_t = 0.99$, $\mathbf{B}_t = 17000$, $\mathbf{A}_c = 1$, $\mathbf{B}_c = 720$ and $l_c = 75$mm. These parameters lead to the uniaxial stress-strain relations presented in Figures 5 and 6.

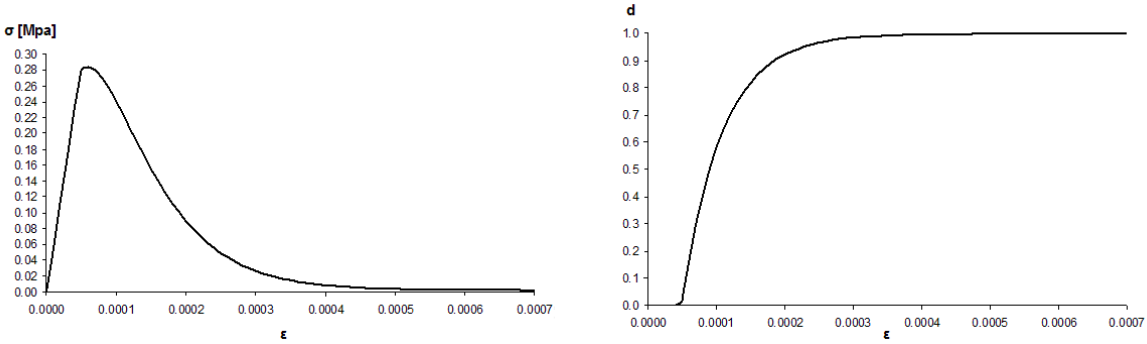

(a) stress-strain (b) damage-strain

Figure 5: Uniaxial tension, Mazars' damage model.

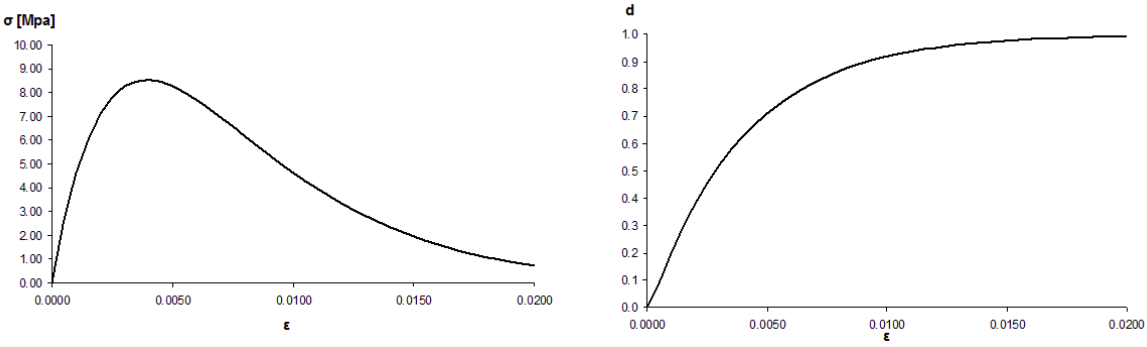

(a) stress-strain (b) damage-strain

Figure 6: Uniaxial compression, Mazars' damagemodel.

The load-displacement diagram obtained is illustrated in Figure 7.

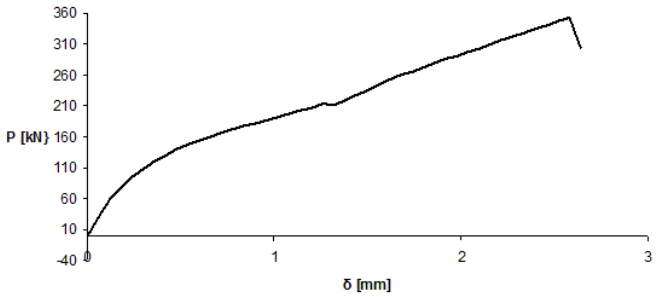

Figure 7: Load-displacement diagram.

When we establish a connection between the load-displacement diagram and the damage distribution (Figure 9), it is perfectly clear that the non-linearity of the load-displacement diagram is a consequence of damage development in the bottom and top boundaries, followed up by the diagonal. These damaged areas are in good agreement with the crack pattern obtained by [Lourenço, 1996] (Figure 8), which has successfully reproduced the experimental crack pattern. Another interesting aspect is that the model was able to capture the damage due to tensile effects and also due to compressive ones (see α_t and α_c distribution in Figure 9).

Even though the modeling strategy adopted was able to capture the damaged areas, it has failed to reproduce the experimental load-displacement diagram, that exhibits a very ductile behavior (Figure 10). This fact can be a consequence of the isotropic hypothesis adopted for the elastic properties and damage process (regular masonry are more likely orthotopic), and of course, the non-calibration of the model.

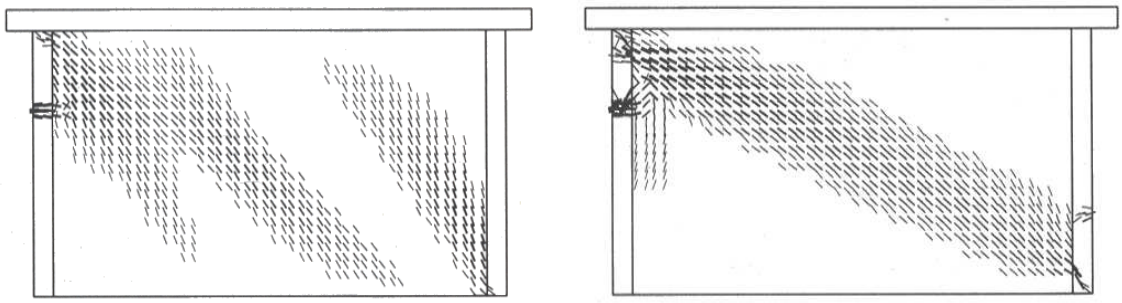

(a) $\delta = 0.2$mm (b) collapse (without the previous crack pattern)

Figure 8: Crack pattern obtained by [Lourenço, 1996].

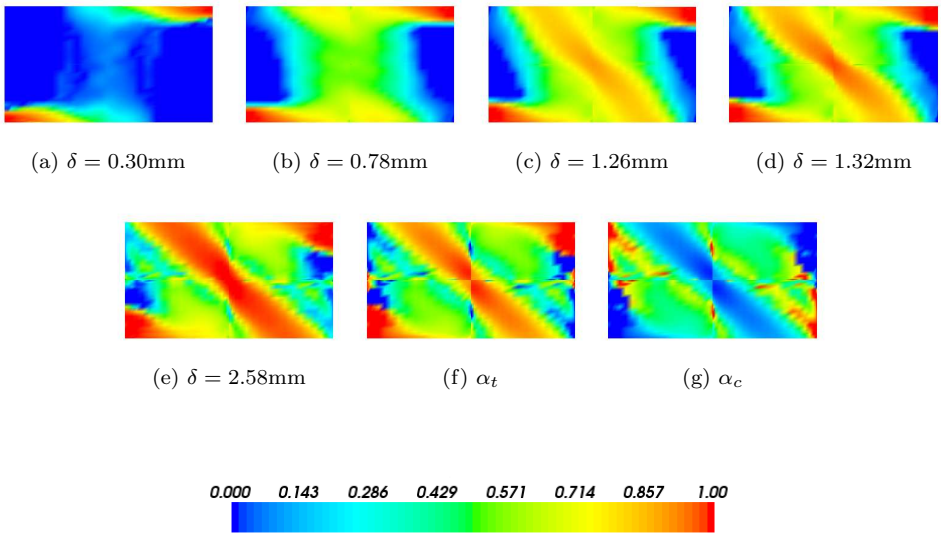

(a) $\delta = 0.30$mm (b) $\delta = 0.78$mm (c) $\delta = 1.26$mm (d) $\delta = 1.32$mm

(e) $\delta = 2.58$mm (f) α_t (g) α_c

(h) colour scale

Figure 9: Damage distribution.

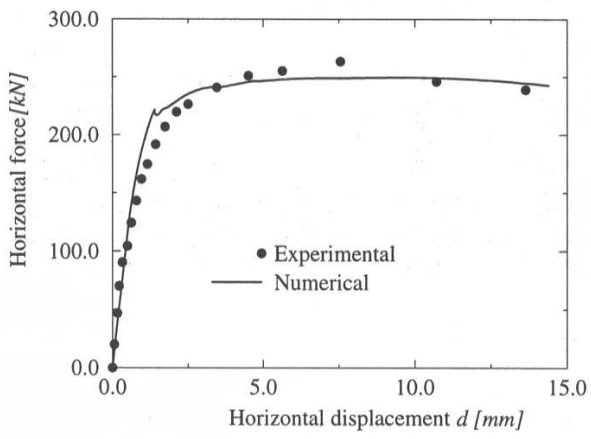

Figure 10: Experimental and Lourenço's numerical load-displacement diagrams.

6.2.1 [Comi and Perego, 2001a] two damage variables model

The ETH Zurich shear wall was also modeled with the two damage variables presented by [Comi and Perego, 2001b]. The model parameters adopted were $\mathbf{E} = 5700$MPa, $\nu = 0.25$, $a_c = 1.4$, $b_c = 8.0$MPa, $k_c = 80.0$MPa^2, $c_c = 4.0$, $(\frac{\sigma_e}{\sigma_0})_c = 0.7$, $d_{0c} = 0.3$, $a_t = 0.002$, $b_t = 3.5$MPa, $k_t = 1.0$MPa^2, $c_t = 4.0$, $(\frac{\sigma_e}{\sigma_0})_t = 1.0$, $d_{0c} = 0.0$ and $l_c = 150$mm, leading to stress-strain relations similar to those illustrated in Figures 5 e 6.

The degree of approximation for the effective stress field is 5, while degree 4 is used in the approximation of the other fields. The finite element mesh used has four equal rectangles.

Unfortunately the model was only able to achieve convergence for some values of l_c and for some meshes. This problem reveals that the software used has numerical problems on determining the two damage variables, when both damage modes are active in the same region (Figure 11).

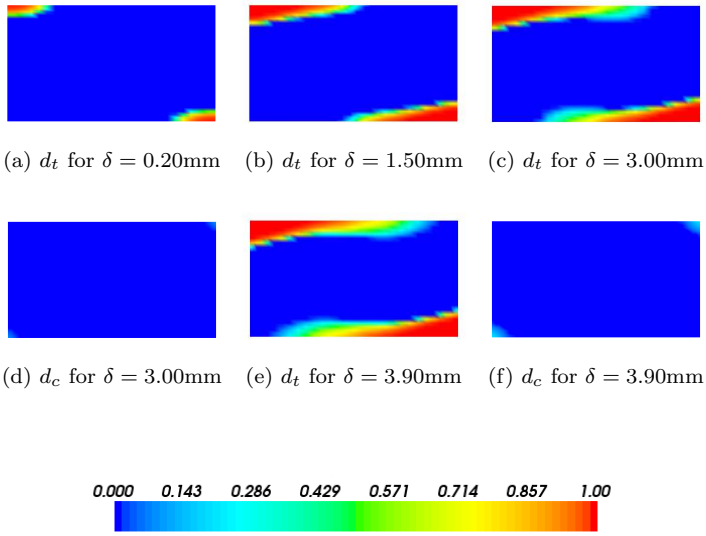

(a) d_t for $\delta = 0.20$mm (b) d_t for $\delta = 1.50$mm (c) d_t for $\delta = 3.00$mm

(d) d_c for $\delta = 3.00$mm (e) d_t for $\delta = 3.90$mm (f) d_c for $\delta = 3.90$mm

(g) colour scale

Figure 11: Damage distribution.

6.3 Cilindrical vault

A cilindrical vault subjected to the action of its self-weight and a point load near quarter span was modeled using a hybrid-mixed stress formulation. The vault thickness is of 130mm, the span of 2000mm and the largeness of 1500mm. [Creazza et al., 2001] has modeled this vault, which also contains three continuous FRP (fibre-reinforced plastic) reinforcements sheets, bonded along the intrados of the vault (Figure 12).

The degree of approximation for the effective stress field is 5, while 4 is the degree used for the other fields. The finite element mesh adopted is illustrated in Figure 12, and the vertical displacement is imposed on the boundary of finite element 10.

The one damage variable model presented by [Comi and Perego, 2001b] is used, adopting the parameters $\mathbf{E} = 1700$MPa, $\nu = 0.25$, $k = 9.22 \times 10^{-5}$MPa, $c = 36.30$, $n = 8.07$ and $l_c = 15$mm, leading to the stress-strain relation presented in Figure 13.

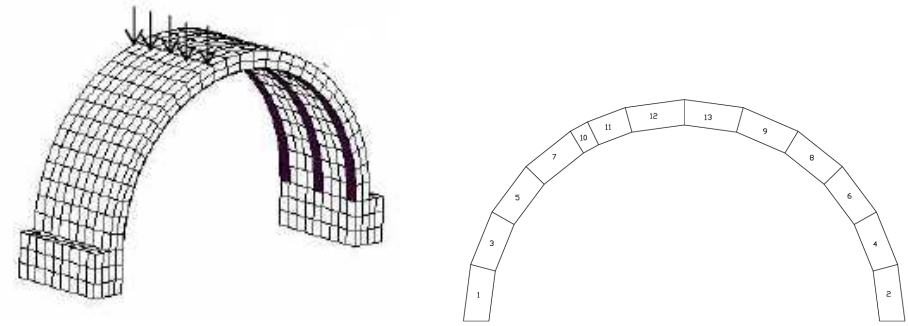

(a) cilindrical vault (b) finite element mesh

Figure 12: Cilindrical vault and finite element mesh.

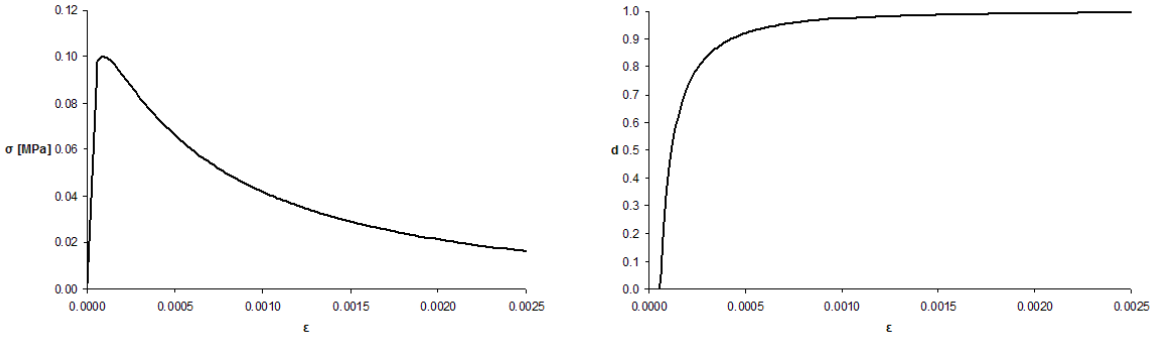

(a) stress-strain (b) damage-strain

Figure 13: Uniaxial tension.

The load-displacement diagram obtained is shown in Figure 14, while the damage distribution is presented in Figure 15.

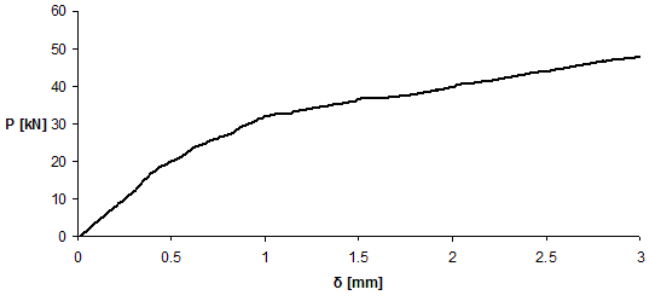

Figure 14: Load-displacement diagram.

The non-linearity of the load-displacement diagram is the consequence of the formation of four damaged areas, which represent the four hinges needed to create the unstable mechanism. This damage distribution is in good agreement with the experimental data, because it was able to predict the location of the four cracked zones responsible for the formation of the unstable mechanism. However, the load-displacement diagram returns to a linear behavior after the formation of the four damaged areas. This is a consequence of the modeling strategy adopted, because no damage is considered for compression, and therefore, the structure is able to equilibrate the loading only with compressive stress states.

For all that has been stated, it is natural to assume that the peak load corresponds to the value for which the structure returns to linear behavior, i.e., 32kN. In order to compare this value, a rigid-plastic analysis was done, using the software developed by [Gago, 2004], assuming that masonry has no tensile strength and has infinite compression strength. Moreover, it is assumed that there are no relative movements between bricks and that the material is non-deformable. Finally, it considered that structure deformation occurs locally by the opening of joints between bricks.

The collapse load obtained in the rigid-plastic analysis was 1.34kN, very far from the value 32kN obtained in the modeling strategy adopted. [Creazza et al., 2001] modeled the cilindrical vault with a isotropic damage model for masonry and a isotropic linear elastic model for FRP. [Creazza et al., 2001] reported that for a displacement value of 1.16mm the model has captured the failure mechanism (which has experimentally happened), but the structure has not collapsed because FRP prevented that happening. Being so, from the point that [Creazza et al., 2001] has captured the failure mechanism of the masonry, the load-displacement obtained by [Creazza et al., 2002] should be linear, because FRP was modeled as a linear elastic material. In fact, [Creazza et al., 2001]'s load-displacement diagram is non-linear and its behavior is like a monotonically increasing function all the way to the collapse. This aspect may tell us that the constitutive relation presented by [Creazza et al., 2001] for masonry is not well calibrated, because the non-linear behavior of FRP is being partially modeled within the masonry properties. Another aspect which may contribute to this huge difference may be that model used smears out units and joints within a continuum material, and it is well known that failure in vaults occurs in the joints, being a extremely located phenomena.

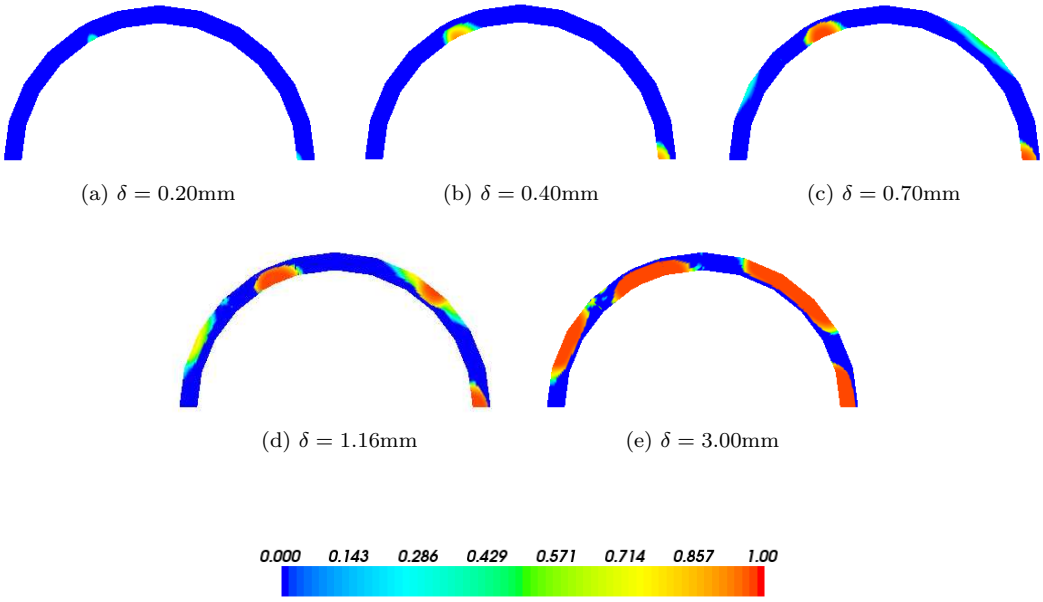

(a) $\delta = 0.20$mm (b) $\delta = 0.40$mm (c) $\delta = 0.70$mm

(d) $\delta = 1.16$mm (e) $\delta = 3.00$mm

(f) colour scale

Figure 15: Damage distribution.

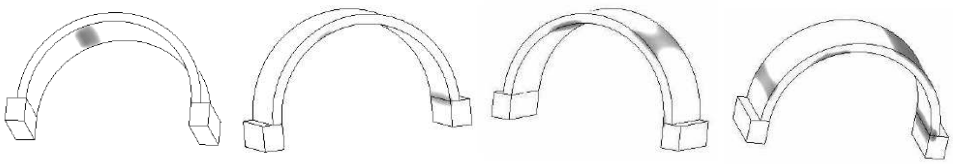

(a) $\delta = 0.40$mm (b) $\delta = 0.45$mm (c) $\delta = 0.71$mm (d) $\delta = 1.16$mm

Figure 16: Damage distribution obtained by [Creazza et al., 2001].

7 Conclusions and future work

The one variable damage model presented by [Comi and Perego, 2001b] is suitable only to model structures in which failure occurs due to pure tension effects. This work confirms that the non-conventional formulations adopted by [Silva, 2006] work well with this constitutive model.

The two damage variables model presented by [Comi and Perego, 2001a] has difficulties to obtain convergence when both damage modes are active on the same region.

The hybrid-mixed stress implementation combined with [Mazars, 1984] model is able to capture almost every phenomena that causes a masonry shear wall to collapse.

Future work may include the vital calibration of the damage models, the implementation of orthotropic damage models (both in elastic regime and in the damage process) and the development of software for 3D analysis and for reinforced masonry structures.

References

Castro, L. M. S. S. (1996). *Wavelets e Séries de Walsh em Elementos Finitos*. Ph. D. thesis, Instituto Superior Técnico, Universidade Técnica de Lisboa.

Comi, C. and U. Perego (2001a). Fracture energy based bi-dissipative damage model for concrete. *International Journal of Solids and Structures*.

Comi, C. and U. Perego (2001b). Numerical aspects of nonlocal damage analyses of concrete structures. *European Journal of Finite Elements*.

Creazza, G., R. Matteazzi, A. Saetta, and R. Vitaliani (2001). Analysis of masonry structures reinforced by frp. In P. Lourenço and P. Roca (Eds.), *Historical Constructions*.

Creazza, G., R. Matteazzi, A. Saetta, and R. Vitaliani (2002). Analyses of masonry vaults: a macro approach based on three-dimensional damage model. *Journal of structural engineering*.

Freitas, J. T. (1989). Duality and symmetry in mixed integral methods of elastotatics. *International Journal for Numerical Methods in Engineering 28*, 1161–1179.

Freitas, J. T., J. M. Almeida, and E. R. Pereira (1999). Non-conventional formulations for the finite element method. *Computational Mechanics 23*, 488–501.

Gago, A. d. S. (2004). *Análise estrutural de arcos, abóbadas e cúpulas - contributo para o estudo do património construído*. Ph. D. thesis, Instituto Superior Técnico, Universidade Técnica de Lisboa.

Lourenço, P. (1996). *Computational strategies for masonry structures*. Ph. D. thesis, Delft University of Technology.

Mazars, J. (1984). *Application de la mécanique de l'endommagement au comportement non linéaire et à la rupture du béton de structure*. Ph. D. thesis, U. Paris.

Oñate, E., A. Hanganu, A. Barbat, S. Oller, R. Vitaliani, A. Saetta, and R. Scotta (1996). Structural analysis and durability assessment of historical constructions using a finite element damage model. In *Structural analysis of historical constructions - possibilities of numerical and experimental techniques*, pp. 189–224. Cimne.

Pereira, E. (1993). *Elementos finitos de tensão - aplicação a análise elásticas de estruturas*. Ph. D. thesis, Instituto Superior Técnico, Universidade Técnica de Lisboa.

Silva, C. and L. Castro (2007). Hybrid-displacement(treftz) formulation for softening materials. *Computers and Structures 85*, 1331–1342.

Silva, M. C. O. M. (2006). *Modelos de Dano em Elementos Finitos Híbridos e Mistos*. Ph. D. thesis, Instituto Superior Técnico, Universidade Técnica de Lisboa.